




Review

Recent Advance and Modification Strategies of Transition Metal Dichalcogenides (TMDs) in Aqueous Zinc Ion Batteries

Tao Li ¹, Haixin Li ¹, Jingchen Yuan ¹, Yong Xia ¹ , Yuejun Liu ¹  and Aokui Sun ^{1,2,*} 

¹ School of Packaging and Materials Engineering, Hunan University of Technology, Zhuzhou 412007, China; 17404200515@stu.hut.edu.cn (T.L.); hxli_2002@163.com (H.L.); jcyuan_66@163.com (J.Y.); xiayong@hut.edu.cn (Y.X.); yjliu_2005@126.com (Y.L.)

² School of Metallurgy and Environment, Central South University, Changsha 410083, China

* Correspondence: aksun@hut.edu.cn

Abstract: In recent years, aqueous zinc ion batteries (ZIBs) have attracted much attention due to their high safety, low cost, and environmental friendliness. Owing to the unique layered structure and more desirable layer spacing, transition metal dichalcogenide (TMD) materials are considered as the comparatively ideal cathode material of ZIBs which facilitate the intercalation/ deintercalation of hydrated Zn²⁺ between layers. However, some disadvantages limit their widespread application, such as low conductivity, low reversible capacity, and rapid capacity decline. In order to improve the electrochemical properties of TMDs, the corresponding modification methods for each TMDs material can be designed from the following modification strategies: defect engineering, intercalation engineering, hybrid engineering, phase engineering, and in-situ electrochemical oxidation. This paper summarizes the research progress of TMDs as cathode materials for ZIBs in recent years, discusses and compares the electrochemical properties of TMD materials, and classifies and introduces the modification methods of MoS₂ and VS₂. Meanwhile, the corresponding modification scheme is proposed to solve the problem of rapid capacity fading of WS₂. Finally, the research prospect of other TMDs as cathodes for ZIBs is put forward.



Citation: Li, T.; Li, H.; Yuan, J.; Xia, Y.; Liu, Y.; Sun, A. Recent Advance and Modification Strategies of Transition Metal Dichalcogenides (TMDs) in Aqueous Zinc Ion Batteries. *Materials* **2022**, *15*, 2654. <https://doi.org/10.3390/ma15072654>

Academic Editor: Satyam Panchal

Received: 10 March 2022

Accepted: 1 April 2022

Published: 4 April 2022

Publisher's Note: MDPI stays neutral with regard to jurisdictional claims in published maps and institutional affiliations.



Copyright: © 2022 by the authors. Licensee MDPI, Basel, Switzerland. This article is an open access article distributed under the terms and conditions of the Creative Commons Attribution (CC BY) license (<https://creativecommons.org/licenses/by/4.0/>).

Keywords: transition metal dichalcogenides; aqueous zinc ion batteries; modification strategy; cathode materials

1. Introduction

Due to the deterioration of the environment and the deficit of fossil energy, it is increasingly important to develop environmentally friendly, sustainable, and renewable energy [1–3]. At present, some renewable energy power generation can meet the requirements of environmental protection and sustainable development, such as solar power, wind power, and tidal power generation, but these energy sources suffer from regional limitations and instability, limiting their wider application. As an important part of energy for sustainable development, electrochemical energy storage has become an active research field in recent decades [4–6]. In the current energy market, lithium-ion batteries (LIBs) are dominant in automobile, medical equipment, portable wearable equipment, and other industries because of their excellent energy density and good environmental performance [7,8]. However, most lithium-ion batteries use organic solvents as electrolytes, which may cause safety problems and increase costs [9–12]. Compared with non-aqueous batteries, aqueous rechargeable batteries have the characteristics of low cost, non-toxicity, and non-flammability, which makes them safer, more environmentally friendly, and more economical [13–15].

In addition to LIBs, many other rechargeable aqueous metal ion batteries have been developed, including sodium ion batteries [16], potassium ion batteries [17], aluminum ion batteries [18], calcium ion batteries [19], and zinc ion batteries. Compared with other rechargeable aqueous metal ion batteries, zinc ion batteries have many advantages [20–22]:

(1) Zinc ion batteries can be directly assembled in the air without inert environment, which can reduce the battery assembly cost. (2) Zinc ions can be electrodeposited reversibly in aqueous solution, so the zinc sheet can be directly used as the anode of the battery. (3) Zinc as anode has a higher theoretical capacity and lower oxidation/reduction potential (-0.76 V) than the standard hydrogen electrode, which indicates that there is a higher open circuit voltage when coupled with cathode. Therefore, in many rechargeable water-based metal ion batteries, the research on aqueous zinc ion batteries is increasingly concerned.

As shown in Figure 1a, the aqueous zinc ion battery (ZIB) is mainly composed of the battery shell, cathode material, anode material, electrolyte, and diaphragm. There are many kinds of cathode materials, including manganese-based materials [23], vanadium-based materials [24], and Prussian blue analogues [25], all of which possess a certain capacity of Zn^{2+} storage. Since the theoretical interlayer spacing of transition metal disulfide compounds is larger than the diameter of Zn^{2+} , Zn^{2+} can be intercalated and deintercalated in TMD material, which also indicates that TMD material is feasible as the cathode of ZIB [26]. At present, few studies have been conducted on TMD as a cathode material of ZIB, and there is not a systematic exposition, which also shows from the aspect that TMD as cathode of ZIB is quite novel. Figure 1b displays the trend of the increasing number of publications, evidencing the increasing attention paid to TMD materials in ZIB. The latest research progress of TMD series materials as cathodes of ZIB in recent years is reviewed in this paper, and several modification methods which can improve the Zn^{2+} storage capacity and structural stability of TMD materials are expounded.

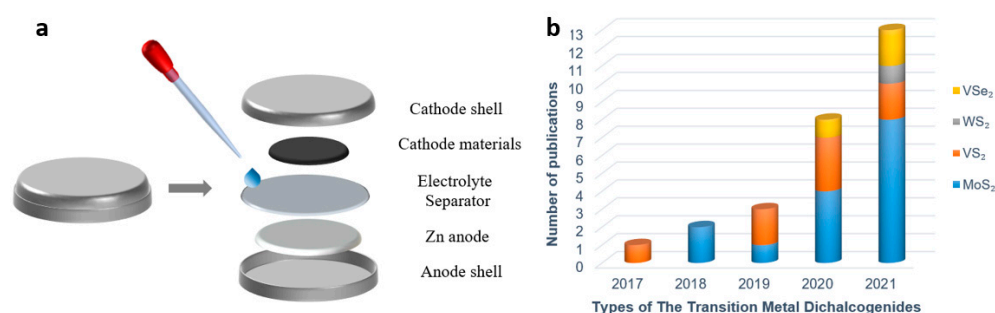


Figure 1. (a) Disassembly diagram of coin-type ZIBs; (b) The trend of publications on TMDs as ZIBs cathode materials.

2. Characterization and Synthetic Methods of TMD

Two-dimensional layered transition metal disulfides (TMDs) generally have X-M-X structure, where M is the transition metal, such as molybdenum, vanadium, tungsten, bismuth, and other metal elements, while X is generally sulfur, selenium, and other elements, as shown in Figure 2a. These layered structures facilitate the transport of various carriers and can also adapt to the volume change during ion insertion. Because of their different chemical composition and unique crystal structure, as well as the fact that the d-orbitals can be filled with different elements, TMDs can be used as functional materials for electronic insulation, semiconductors, and superconductivity [27].

Among all TMDs materials, molybdenum disulfide (MoS_2) has received extensive attention as a typical representative. Molybdenum disulfide is composed of two layers of sulfur atoms and one layer of molybdenum atoms, with the metal molybdenum layer interposed between the two sulfur layers, alternately stacked to form a sandwich-like structure. The sulfur atoms are bound together by van der Waals force, while the S-Mo-S atoms are linked by strong covalent bonds [28,29]. MoS_2 not only has a layered structure, but also has different phases (1T, 2H, and 3R), and each phase also has different physical properties and chemical characteristics [30]. As shown in Figure 2b, MoS_2 in 2H and 3R phases both demonstrate the triangular prismatic coordination of Mo atoms, and 2H- MoS_2 is very stable because of the two layers of units stacked in hexagon symmetry. Meanwhile, 3R- MoS_2 has rhombus symmetry, and each unit has three layers. On the contrary, the Mo

atoms of 1T-MoS₂ (metal phase) are octahedral coordinated and most unstable [31,32]. VS₂ is also a common material in TMDs, where the sulfur and vanadium layers are stacked together in a sandwich-like structure by van der Waals force interactions [33,34]. Due to the large interlayer spacing, VS₂ has great potential in the intercalation/deintercalation of ions, such as Li⁺, Na⁺, Zn²⁺, Mg²⁺, and Al³⁺ [35–37].

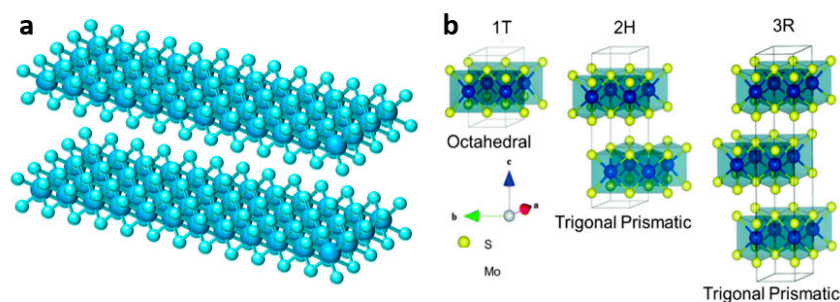


Figure 2. (a) Illustration of TMD structure; (b) Atomic structures of 1T-, 2H-, and 3R-MoS₂ [31].

In order to obtain layered and nanoflower-like sulfide materials, TMD materials are generally prepared by hydrothermal and solvothermal methods. The synthetic methods of TMD materials as ZIB cathode are summarized in Table 1.

Table 1. Fabrication methods, precursors and synthesis conditions of TMDs as ZIBs cathode.

Products	Method	Precursors	Temperature	Duration	Ref
MoS _{2-x}	Hydrothermal	(NH ₄) ₆ Mo ₇ O ₂₄ ·4H ₂ O, TAA	200 °C	18 h	[38]
E- MoS ₂	Hydrothermal	Na ₂ MoO ₄ , CS(NH ₂) ₂ , carbon cloth, glucose, HCl	190 °C	24 h	[39]
MoS ₂ -O	Hydrothermal	(NH ₄) ₆ Mo ₇ O ₂₄ ·4H ₂ O, thiourea	180 °C	24 h	[40]
MoS ₂ ·nH ₂ O	Hydrothermal	(NH ₄) ₆ Mo ₇ O ₂₄ ·4H ₂ O, thiourea	170 °C	24 h	[41]
MoS ₂ /PANI	Solvothermal	Na ₂ MoO ₄ , thiourea, C ₁₇ H ₃₃ CO ₂ Na, ethanol, OA, HCl	180 °C	24 h	[42]
MoS ₂ @CNTs	Hydrothermal	Na ₂ MoO ₄ ·2H ₂ O, thiourea, CNTs, glucose	200 °C	24 h	[43]
MoS ₂ -160	Hydrothermal	(NH ₄) ₆ Mo ₇ O ₂₄ ·4H ₂ O, thiourea	160 °C	24 h	[44]
VS ₂	Hydrothermal	NH ₄ VO ₃ , TAA, NH ₃ ·H ₂ O	180 °C	20 h	[45]
VS ₂ @SS	Hydrothermal	NH ₄ VO ₃ , TAA, NH ₃ ·H ₂ O, stainless steel mesh	180 °C	10 h	[46]
rGO-VS ₂	Solvothermal	VO(acac) ₂ , cysteine, GO, NMP	200 °C	8 h	[47]
VS ₂ @VOOH	Hydrothermal	V ₂ O ₅ , TAA, NH ₃ ·H ₂ O	180 °C	18 h	[48]
VS ₂ ·NH ₃	Solvothermal	VO(acac) ₂ , TAA, NMP	200 °C	24 h	[49]
VS ₂ /VO _x	Solvothermal	Na ₃ VO ₄ ·12H ₂ O, TAA, ethylene	180 °C	20 h	[50]
1T-WS ₂	Solvothermal	WCl ₆ , TAA, DMF	200 °C	24 h	[51]
VSe ₂	Chemical Liquid Phase Synthesis	VO(acac) ₂ , Se powder, OAm	330 °C	5 h	[52]

3. TMDs as ZIBs Cathode

Layered MoS₂, VS₂, WS₂, and VSe₂ have been proven to be feasible cathode materials for ZIB in recent years. MoS₂ is the earliest and most extensively material studied in ZIB owing to its unique layered structure and different phases. However, compared with manganese-based materials and vanadium-based materials, TMDs have lower conductivity and larger capacity changes, which will lead to the lower rate performance and poor cycle performance of electrode materials during charge and discharge, which is also the biggest challenge for TMDs materials. In order to improve the electrochemical performance of TMDs, different modification strategies of TMDs were designed. In this section, the research progress of MoS₂, VS₂, WS₂, and VSe₂ materials as cathode materials for ZIB is described, and various modification methods of MoS₂ and VS₂ materials are discussed and summarized.

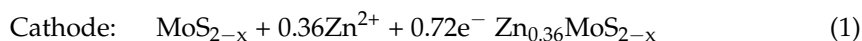
3.1. MoS₂ and Modification

Liu et al. [53] did not obtain obvious redox peaks in CV curves of MoS₂ and WS₂, indicating that it is difficult for MoS₂ and WS₂ to store zinc ions. The measured cyclic discharge capacities provided by MoS₂ and WS₂ were 18 mAh·g⁻¹ and 22 mAh·g⁻¹, respectively, and the EDS images of MoS₂ and WS₂ in the fully discharged state also had low zinc contents, so their conclusions showed that MoS₂ and WS₂ materials were not suitable as cathode materials for ZIB. The electrochemical performance of unmodified MoS₂ in ZIB is undesirable, such that more and more scholars have paid attention to the modified MoS₂ as the cathode material of ZIB.

3.1.1. Defect Engineering

Defect engineering is used to change the surface properties and structure of TMDs to improve the electrochemical performance, which is undoubtedly a preferable modification strategy. The possible vacancy defects in TMDs consist of sulfur vacancies, transition metal vacancies, edge vacancies, and holes in the crystal lattice [54–56]. The main effects of defects on electrode materials are divided into three types: (1) More storage and adsorption sites of foreign ions are provided to improve the battery capacity. The introduction of defects increases the number of active sites significantly, which improves the electrochemical performance. (2) It changes the local structure and charge distribution on the surface of electrode materials, which can improve the conductivity, cycle stability, and rate performance of electrode materials. (3) Defects can make the structure more flexible and stable when external ions are intercalated and deintercalated. Therefore, the introduction of defects in the crystal structure of TMDs and the selection of appropriate chemical modification molecules or groups using the defect sites constructed on the surface of TMDs can improve the electrical conductivity, reversible capacity, and initial Coulombic efficiency (ICE) and enhance the reversibility of Zn²⁺ intercalation/de intercalation, thus improving the electrochemical performance of TMD electrode materials in ZIB.

For example, Xu et al. [38] designed the first MoS_{2-x}/Zn cell and confirmed that defect engineering could be used to enhance the Zn storage capacity of MoS₂. They predicted that the edge vacancies and sulfur vacancies were the main adsorption sites of Zn²⁺ by DFT, while the original surface was inert in storing Zn²⁺ due to the lack of these vacancies. As shown in Figure 3, owing to the absence of some chalcogen atoms, there is a large number of vacancies existing in the neatly arranged sulfur layer. These vacancies include edge vacancies and sulfur vacancies, which can easily accommodate more Zn²⁺ for intercalation, resulting in a significant increase in the reversible capacity of ZIBs. Such a layered nanostructure with rich defects can also reduce the diffusion energy barrier and significantly increase the diffusion rate of Zn ions [57]. Figure 4a shows that the capacity of defect-free MoS₂ nanosheets is very low at a current density of 100 mA·g⁻¹, while the defect-rich MoS₂ nanosheets provide a high reversible capacity of 135 mAh·g⁻¹. After 1000 cycles at a current density of 1000 mA·g⁻¹, the defect-rich MoS₂ electrode still delivers a high reversible capacity of 88.6 mAh·g⁻¹ with a capacity retention of 87.8%. The electrochemical reaction mechanism of the MoS_{2-x}/Zn battery at cathode and anode can be expressed as:



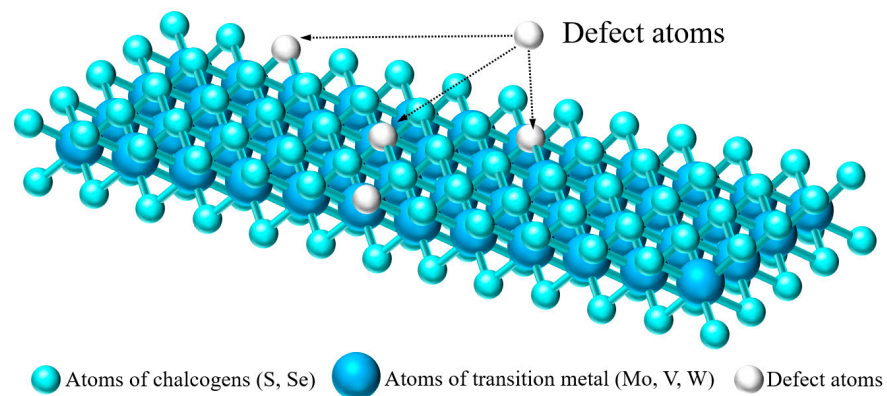


Figure 3. Defect atoms in TMDs single layer.

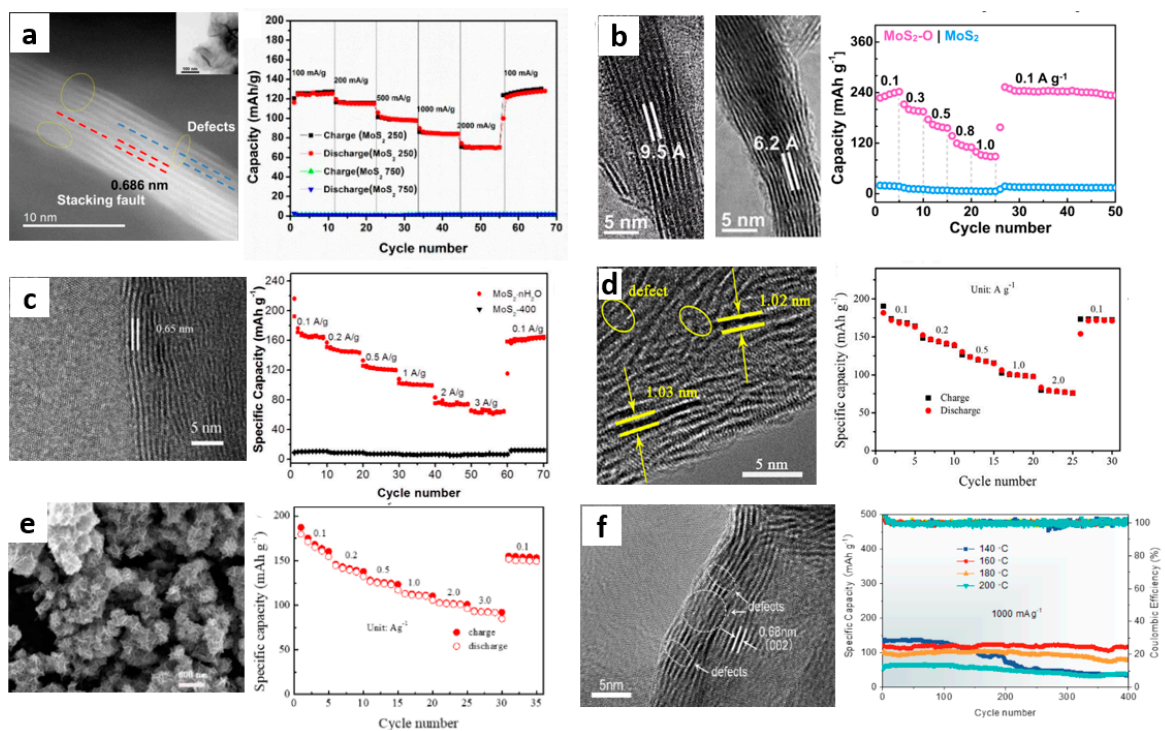


Figure 4. (a) HRTEM image of the defect-rich MoS_2 and its rate performance [38]; (b) HRTEM images of oxygen incorporated MoS_2 (left showing oxygen incorporated MoS_2 , right showing pristine MoS_2) and the rate performance of oxygen incorporated MoS_2 [40]; (c) HRTEM image of $\text{MoS}_2\cdot n\text{H}_2\text{O}$ and the rate performance of $\text{Zn}/\text{MoS}_2\cdot n\text{H}_2\text{O}$ batteries [41]; (d) HRTEM image of the $\text{MoS}_2/\text{PANI}-150$ hybrid and its rate performance [42]; (e) SEM image and rate performance of the $\text{MoS}_2@\text{CNTs}$ hybrid electrode [43]; (f) HRTEM image of MoS_2-160 , and cycling performances at current densities of 1.0 A g^{-1} of MoS_2 at various temperatures [44].

3.1.2. Interlayer Engineering

The non-bonded characteristics of 2D layered materials with unique vdW gaps between adjacent atomic layers allows the insertion of atoms, ions, and molecules without breaking covalent bonds through a chemical intercalation process, thus changing the physical and chemical properties of the material [58]. TMDs are generally composed of 2D single-molecule layers combined with van der Waals forces and weak chemical bonds stacked along the direction perpendicular to the layers, a structure that has a larger specific surface area and is also conducive to the insertion of small intercalators, such as ions and molecules. Figure 5 shows that the insertion of external ions can expand the interlayer spacing of TMDs.

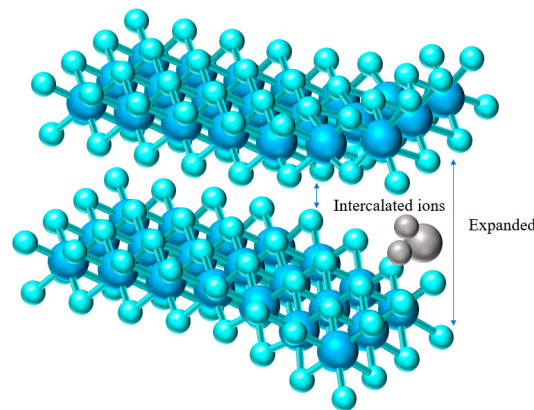
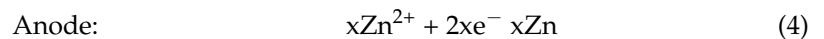


Figure 5. Ion Intercalation in single layer TMDs structure.

Li et al. [39] prepared expanded interlayer distance E-MoS₂ nanosheets vertically aligned on carbon fiber cloth by a one-step glucose-assisted hydrothermal method as cathode materials for ZIB. The layer spacing of commercial MoS₂ is 0.62 nm, while the interlayer spacing of E-MoS₂ nanosheets is 0.70 nm. The increased interlayer spacing is due to the incorporation of hydrated Na⁺ and NH₄⁺ into the MoS₂ crystal framework during the hydrothermal reaction. The E-MoS₂ electrode also showed good performance with a specific capacity of 202.6 mAh·g⁻¹ and a specific energy density of 148.2 Wh·kg⁻¹ at 0.1 A·g⁻¹ as well as a capacity retention rate of 98.6% after more than 600 cycles with good cycling stability. The electrochemical reaction mechanism of the cathode and anode of E-MoS₂/Zn battery is expressed as:



Liang et al. [40] made MoS₂-O to store Zn ions more efficiently by adjusting the interlayer spacing and designing hydrophilicity tuning engineering. A small amount of oxygen (5%) was added to MoS₂, and the incorporation of oxygen improved the hydrophilicity of MoS₂-O and made it possible for water to intercalate in MoS₂-O, which also increased the interlayer spacing of MoS₂-O from 0.62 to 0.95 nm, as shown in Figure 4b. Furthermore, if a diffusing hydrated Zn²⁺ were to diffuse through a narrow void separation in MoS₂ (S to S layer separation), i.e., 0.31 nm, instead of the 0.62 nm, i.e., Mo to Mo layer separation, interlayer engineering becomes even more crucial. As a result, the incorporation of oxygen increased the diffusion rate of Zn²⁺ by three orders of magnitude and the storage capacity of Zn²⁺ was increased by 10 times. When the current density is 100 mA·g⁻¹, the capacity reaches 232 mAh·g⁻¹, which is higher than that of MoS₂-based electrode materials in other ZIB.

Unusually, Zhang et al. [41] designed a material with crystalline water introduced into MoS₂ nanoflowers as cathode materials for ZIB. The MoS₂·nH₂O nanoflowers obtained by the one-step hydrothermal method are composed of layered nanosheets with low stacking height and uniform distribution, as shown in Figure 4c. The insertion of crystalline water not only increases the interlayer distance of MoS₂ to 0.65 nm, but also shields the electrostatic interaction between zinc ions and matrix materials, and lubricates and increases the diffusion ion channels as a way to promote the migration of Zn²⁺. Under the synergistic effect of crystal water lubrication and nanoflower structure, the reversible capacity of MoS₂·nH₂O was 165 mAh·g⁻¹ at 0.1 A·g⁻¹. At the high current density of 2 A·g⁻¹, the capacity retention rate after 800 cycles was 88%.

Huang et al. [42] first designed a molybdenum disulfide/polyaniline (MoS₂/PANI) hybrid material with overlapping heterostructures as an excellent cathode for ZIB. The MoS₂/PANI prepared by the hydrothermal method is a micro-nanoflower assembled by some ultra-thin wrinkled nanosheets with a layer spacing of 1.03 nm, as shown in Figure 4d.

An appropriate amount of PANI was inserted into the MoS₂ matrix, thus expanding the interlayer spacing and shielding the electrostatic interaction between some Zn²⁺ and MoS₂ substrates. The intercalation of polyaniline not only expands the Zn²⁺ diffusion channel, but also reduces the band gap between the conduction band and the valence band of MoS₂, which improves the charge transfer efficiency. Compared with the original MoS₂, the zinc storage performance of the MoS₂/PANI hybrid cathode was significantly improved. At a current density of 1.0 A·g⁻¹, it provides a high reversible capacity of 106.5 mAh·g⁻¹ and maintains 86% capacity after 1000 cycles. This also provides a modification strategy for developing other TMD materials as good cathode materials for ZIB.

3.1.3. Hybridization

The conductivity of TMDs is poor, which limits the diffusion power of ions. In electrochemical energy storage, carbon nanotubes, carbon fiber cloth, and graphene are the most commonly used hybrid materials. Carbon nanotubes and graphene materials have unique structures, high electrical conductivity, good mechanical properties, and large specific surface areas [59,60]. As shown in Figure 6, coating with a certain material or hybridizing with carbon nanotubes, carbon cloth, and graphene on the surface of the TMD can increase the surface area and charge transfer ability of the material to improve the electrochemical performance of the composite.

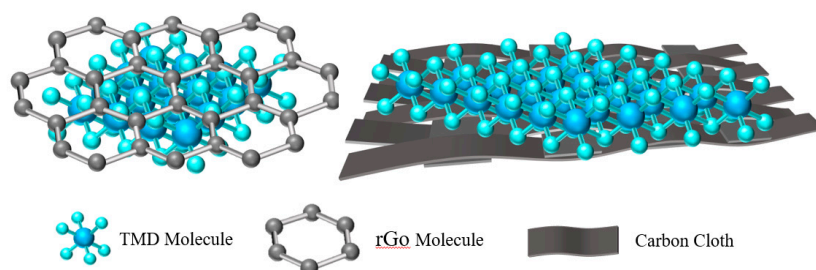


Figure 6. Modification of TMDs by Hybrid Engineering.

Huang [43] dispersed multi-walled carbon nanotubes in aqueous solution mixed with glucose and deionized water, and prepared ultra-thin MoS₂ nanosheets with expanded layer spacing directly grown on the surface of carbon nanotubes (CNTs) by a one-step hydrothermal method (as shown in Figure 4e) as the ZIB cathode material. When the interlayer spacing of MoS₂ increases to 1.0 nm, the increase of interlayer spacing reduces the diffusion energy barrier of Zn²⁺ between layers, and the main chain of CNTs promotes the electron transfer of Zn²⁺ between layers. More importantly, the layered structure hinders the aggregation of MoS₂ nanosheets, increases the surface area, and provides a large number of active sites for electrochemical reactions. At the current density of 0.1 A·g⁻¹, the reversible capacity of the MoS₂@CNTs electrode was about 180.0 mAh·g⁻¹. When the current density increases to 3 A·g⁻¹, it can maintain 51.7% capacity, and after 500 cycles (the current density is 1.0 A·g⁻¹) it can maintain 80.1% capacity. Therefore, MoS₂@CNTs as cathode can provide high reversible capacity and good cycle stability for ZIB.

3.1.4. Phase Engineering

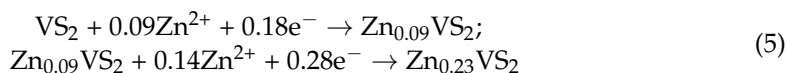
Phase engineering has been proven to be an effective method to regulate the electrochemical performance of TMDs [61]. According to different stacking methods, the materials can be divided into three bulk phases: 1T, 2H and 3R. The cell of 1T phase is octahedral, and the cell of 2H phase is prismatic. Due to different atomic configurations, single-layer TMD materials can also exist in three different forms of 1T, 2H, and 3R, respectively. MoS₂ is a typical TMD which has different phase structures, different metal coordination geometries, different stacking sequences, and different properties. For example, the natural bulk MoS₂ crystal has a 2H phase with triangular prism coordination geometry, but the coordination of

molybdenum and sulfur atoms is octahedral in 1T phase which shows metallicity [62,63]. In fact, the conductivity of 1T phase MoS₂ is about 105 times higher than that of the 2H phase MoS₂ corresponding to semiconductor [64,65]. It can be reasonably speculated that MoS₂ with different phases exhibits different properties in application. Phase engineering has also been proven to be an effective strategy to regulate the catalytic activity of MoS₂ [66].

For example, Liu et al. [44] prepared MoS₂ with different phases by regulating the reaction temperature of the hydrothermal reaction, and most samples showed a flower-like structure of self-assembled nanosheets. As the synthesis temperature decreases, the interlayer spacing of MoS₂ increases from 0.62 nm to 0.68 nm, as shown in Figure 4f. Different from MoS₂ nanosheets corresponding to 2H, MoS₂ nanosheets with high 1T phase content (about 70%) have excellent specific capacity, and the reason for this is that the Zn²⁺ diffusion barrier of 1T-MoS₂ is much lower than that of 2H-MoS₂. At a current density of 1.0 A·g⁻¹, the reversible capacity of 1T-MoS₂ is about 140 mAh·g⁻¹, but the capacity decreases rapidly after 100 cycles. However, the capacity attenuation of 2H-MoS₂ can be ignored after 400 cycles, showing good cycle performance. How to make MoS₂ show excellent specific capacity and maintain stable cycle performance is still worth exploring.

3.2. VS₂ and Modification

In recent years, vanadium disulfide (VS₂) based nanomaterials have become potential electrode materials for various energy storage batteries due to their highly controllable structure and chemical composition. The VS₂ layer shows metallicity and has a considerable electronic state at the Fermi level, which is conducive to promoting electron and electrochemical activity [67]. At present, using VS₂ as the cathode of ZIB is still considered to be a relatively new method. So far, there are only a few reports on VS₂ as the cathode of ZIB. For example, He et al. [45] firstly synthesized rose-like VS₂ nanoflowers assembled by nanosheets with diameter of 5–8 μm and thickness of 50–100 nm, whose interlayer spacing is 0.576 nm, as shown in Figure 7a. These nanosheets can realize the intercalation/deintercalation of Zn²⁺ in VS₂ nanosheets. At a current density of 0.05 A·g⁻¹, VS₂ nanosheets have a high capacity of 190.3 mAh·g⁻¹ and an energy density of 123 Wh·kg⁻¹. The capacity retention rate reached 98.0% after 200 cycles at a current density of 0.5 A·g⁻¹, which confirmed the feasibility of VS₂ as the cathode of ZIB. They summarize the electrochemical reactions occurring in the cathode of Zn/VVS₂ batteries, as shown in Equation (5):



In other reports, VS₂ was modified to obtain electrode materials with better electrochemical performance. Consistently, we reviewed the research progress of modified VS₂ as electrode material for ZIB and summarized two corresponding modification strategies in this section.

3.2.1. Hybridization

Jiao et al. [46] synthesized hierarchical 1T-VS₂ directly on stainless steel mesh (VS₂@SS) by the hydrothermal method. The prepared VS₂ was composed of bending nanosheets with a transverse size of 5–8 μm, forming a highly layered network flower structure from Figure 7b. There is a large number of interlayer channels for electrolyte penetration in VS₂ nanoflowers, which enhances the contact area between electrolyte and VS₂ and promotes the transmission of electrons and ions. Therefore, the VS₂@SS electrode with VS₂ loading of 4–5 mg·cm⁻² has a high capacity of 198 mAh·g⁻¹ at a current density of 50 mA·g⁻¹. After 2000 cycles at a current density of 2 A·g⁻¹, the capacity retention rate was about 80%, showing a superior cycle life. When the mass load of VS₂ is about 11 mg·cm⁻², the electrode can maintain 90% capacity in 600 cycles (only 0.017% loss per cycle), which indicates that the stability of the composite structure is enhanced after the hybrid of TMD material and SS.

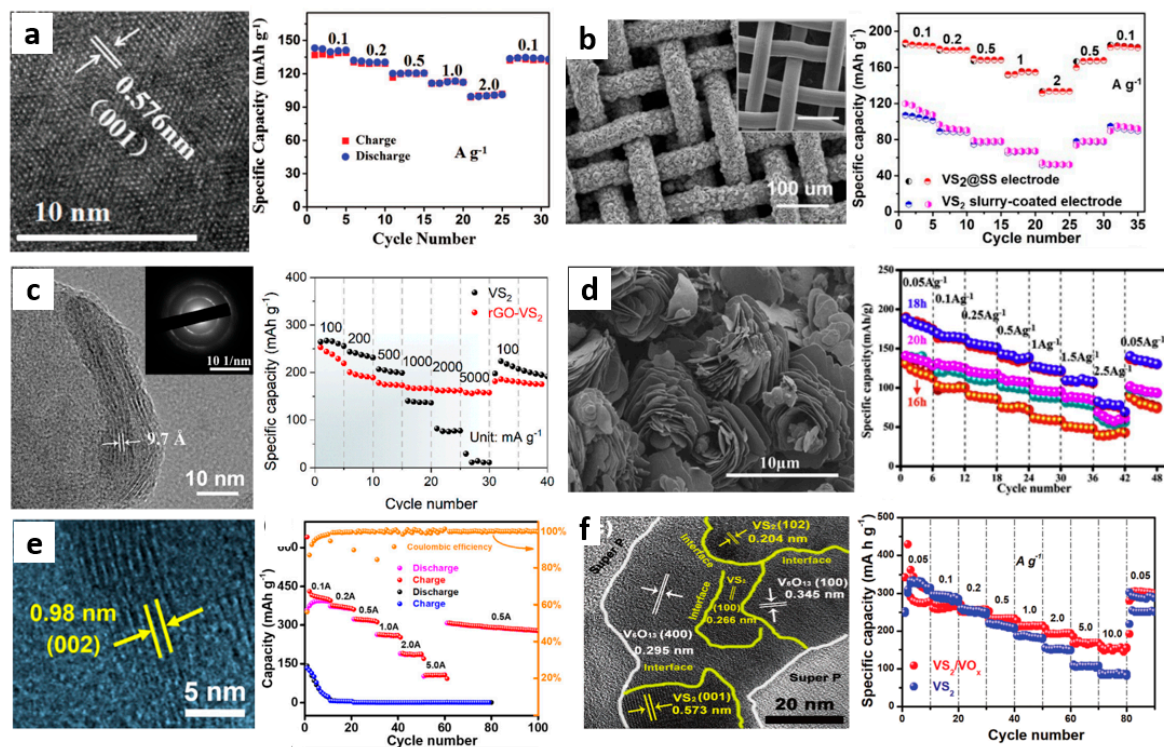


Figure 7. (a) HR–TEM image and rate performance of layered VS_2 [45]; (b) SEM image of VS_2 grown on SS mesh and rate performance of VS_2 @SS electrode [46]; (c) HRTEM image and rate performance of the rGO– VS_2 composites [47]; (d) SEM image and rate performance of the VS_2 @VOOH–18h [48]; (e) HRTEM image and rate performance of $\text{VS}_2 \cdot \text{NH}_3$ electrode [49]; (f) TEM image and rate capability of in–situ electrochemical oxidation formed VS_2/VO_x [50].

Graphene and reduced graphene oxide (rGO) are idealized cathode materials with large specific surface area, excellent electrical conductivity, and excellent mechanical elasticity [68]. In addition, the end-functional group surface of rGO further provides the possibility of strong interface coupling between the active material and the conductive skeleton, and it also realizes the rapid charge transfer and high structural stability against repeated electrochemical cycles [69,70]. Due to the unique layered structure and large specific surface area of graphene and VS_2 , the electrochemical performance of the electrode can be further improved by hybridizing graphene and VS_2 . For example, Chen et al. [65] synthesized vertically grown ultra-thin VS_2 nanosheets (rGO- VS_2) on graphene sheets by the solvothermal method. The interlayer distance of these ultrathin VS_2 nanosheets is about 0.97 nm, as shown in Figure 7c, which is much larger than that of commercial VS_2 crystals (0.575 nm). They also calculated that the surface area of rGO- VS_2 was $34.2 \text{ m}^2 \cdot \text{g}^{-1}$, which was larger than that of commercial VS_2 ($26.5 \text{ m}^2 \cdot \text{g}^{-1}$), indicating that the introduction of graphene increased the specific surface area of the composites. VS_2 nanosheets are closely connected with graphene, which can effectively prevent the dissolution of VS_2 and improve the cycle stability of the battery. Therefore, when the current density is $0.1 \text{ A} \cdot \text{g}^{-1}$, it has a high capacity of $238 \text{ mAh} \cdot \text{g}^{-1}$. At a high current density of $5 \text{ A} \cdot \text{g}^{-1}$, the capacity is $190 \text{ mAh} \cdot \text{g}^{-1}$, and the capacity retention is over 93% after 1000 cycles.

Metal oxides, polymers, C_3N_4 , and MXene can also be hybridized with TMD materials [71–73]. Pu et al. [48] prepared a rose-like VS_2 @VOOH material with hydrophilic VOOH coating for the first time. The size of VS_2 @VOOH is about $10 \mu\text{m}$ and a large number of nanosheets are assembled into uniform rose-like morphology, as shown in Figure 7d. Hydrophilic VOOH coating is conducive to the penetration of electrolyte in ZIB, and the structure is still intact even after O–H is exchanged with water in VOOH. Their research also showed that the O–H bond in VOOH could not only improve the permeation of electrolyte to the electrode, but also reduce the possibility of vanadium dissolution. Therefore, after

350 cycles at a current density of $1.5 \text{ A}\cdot\text{g}^{-1}$, the specific capacity of $\text{VS}_2@\text{VOOH}$ composite can reach $107.5 \text{ mAh}\cdot\text{g}^{-1}$. Even after 400 cycles at a current density of $2.5 \text{ A}\cdot\text{g}^{-1}$, the $\text{VS}_2@\text{VOOH}$ material still maintained a specific capacity of $91.4 \text{ mAh}\cdot\text{g}^{-1}$, which further verified the potential of the modified VS_2 as a ZIB cathode.

3.2.2. In Suit Electrochemical Oxidation

Electrochemical oxidation, as a feasible and multi-purpose strategy, has been proven to enhance the electrochemical behavior of low-valent active substances relative to evolutionary forms and newly formed high-active substances [74–77]. As shown in Figure 8, electrochemical oxidation of the inserted ions into the corresponding oxides without changing the position of the ion insertion into the TMD can provide more active sites or enhance the hydrophilicity of the ions, which is beneficial to the diffusion of Zn^{2+} and the expansion of the TMD layer spacing. Yang et al. [49] prepared a hollow spherical $\text{VS}_2\cdot\text{NH}_3$ material with layer spacing expansion as the cathode of ZIB. The $\text{VS}_2\cdot\text{NH}_3$ hollow flower ball assembled by nanosheets has a porous structure, and the expanded layer spacing is 0.98 nm , as shown in Figure 7e. They found that during the first charge process, the expanded $\text{VS}_2\cdot\text{NH}_3$ transformed into $\text{V}_2\text{O}_5\cdot\text{nH}_2\text{O}$ with a layer spacing of 1.21 nm after electrochemical oxidation. Then, Zn^{2+} was intercalated/deintercalated in $\text{V}_2\text{O}_5\cdot\text{nH}_2\text{O}$ with large interlayer spacing, which provided high capacity and good stability for subsequent charge–discharge cycles. When the current density is $0.1, 0.2, 0.5, 1.0, 2.0,$ and $5.0 \text{ A}\cdot\text{g}^{-1}$, the capacity of the $\text{Zn}/\text{VS}_2\cdot\text{NH}_3$ battery is $390, 372, 320, 260, 189,$ and $107 \text{ mAh}\cdot\text{g}^{-1}$, respectively, which is much higher than the VS_2 -based cathode of other ZIB previously reported. It is worth noting that the electrode formed by in-situ electrochemical oxidation into $\text{V}_2\text{O}_5\cdot\text{nH}_2\text{O}$ reached an amazing 110% capacity retention compared with the initial capacity after 2000 cycles at a high current density of $3 \text{ A}\cdot\text{g}^{-1}$.

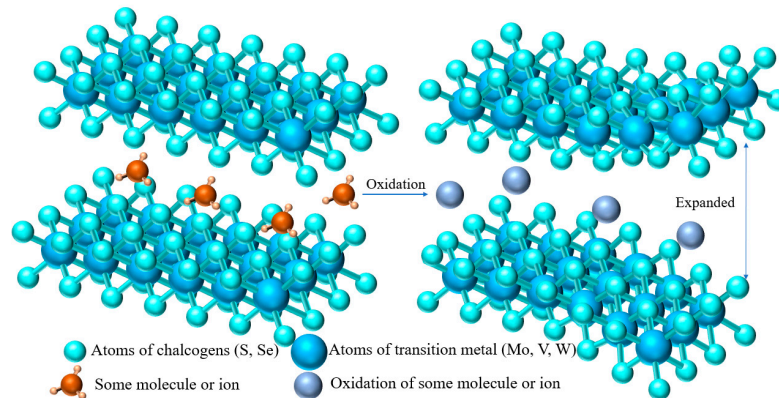


Figure 8. Modification of TMDs by in-situ electrochemical oxidation.

Yu et al. [50] first used the in situ electrochemical pretreatment of VS_2 in aqueous medium and obtained VS_2/VO_x heterostructures as cathode materials for ZIB. The fluffy VO_x nanosheets are uniformly grown on VS_2 , forming an interwoven porous electrode rich in VS_2 and VO_x heterostructures. The VS_2/VO_x heterostructure combines the high conductivity of VS_2 and the high chemical stability of VO_x , which is conducive to regulating the intercalation of guest ions and improving the chemical stability of the VS_2 skeleton. The step-by-step insertion of Zn^{2+} changed the buffer volume, making the reaction kinetics faster and more reversible. As shown in Figure 7f, the VS_2/VO_x electrode maintains 75% high capacity in 3000 cycles at a current density of $1 \text{ A}\cdot\text{g}^{-1}$. After 1000 cycles, VS_2/VO_x still maintained the original crystal structure and nanosheet morphology, which again proved that the VS_2/VO_x heterostructure had high reversibility. As a consequence, the design of TMD heterostructures by in situ electrochemical oxidation provides a new strategy for the efficient energy storage of ZIB.

3.3. WS₂ and Modification

WS₂ is a natural metal sulfide, where the S atom is located in the lattice position of the closely packed hexagonal structure. The plane where the W atom lies is sandwiched between two S layers and each W atom is coordinated with the S atom. The W layer and the S layer are stacked together through a weak van der Waals effect to form a prismatic structure [78,79]. The theoretical layer spacing of WS₂ is 0.618 nm, while the diameter of Zn²⁺ is only 0.404–0.43 nm. Theoretically, it can also be used as the electrode material of the energy storage battery, but there are few reports on it as the ZIB cathode material. A report [53] on WS₂ pointed out that the interlayer spacing of commercial WS₂ was insufficient, and the inherent conductivity of Zn²⁺ for reversible intercalation between layers was low, which indicates that the storage capacity of commercial WS₂ for Zn²⁺ was poor. Another reason for this is that 2H-WS₂ has a large Zn²⁺ intercalation barrier, which seriously hinders the diffusion of Zn²⁺ to electrode materials.

Tang et al. [51] proved for the first time that 1T-WS₂ nanosheets are a promising candidate cathode material for ZIB. Thus, 1T phase WS-200 is stacked by ultrathin nanosheets, and the interlayer spacing is expanded from 0.618 nm to about 0.90 nm. After the introduction of 1T-WS₂, the capacity of an almost inactive Zn/WS₂ battery increased by eight times, and the reversible capacity was 179.99 mAh·g⁻¹ at a current density of 200 mA·g⁻¹. However, WS₂ has the problem of rapid capacity degradation in the long cycle at different current densities from Figure 9a. Their explanation for this phenomenon is that the layered WS₂ structure collapsed and dissolved, and some 1T-WS₂ dissolved in the electrolyte during the intercalation/deintercalation of Zn²⁺, which provides a research direction for improving the reversible capacity and cycle stability of WS₂.

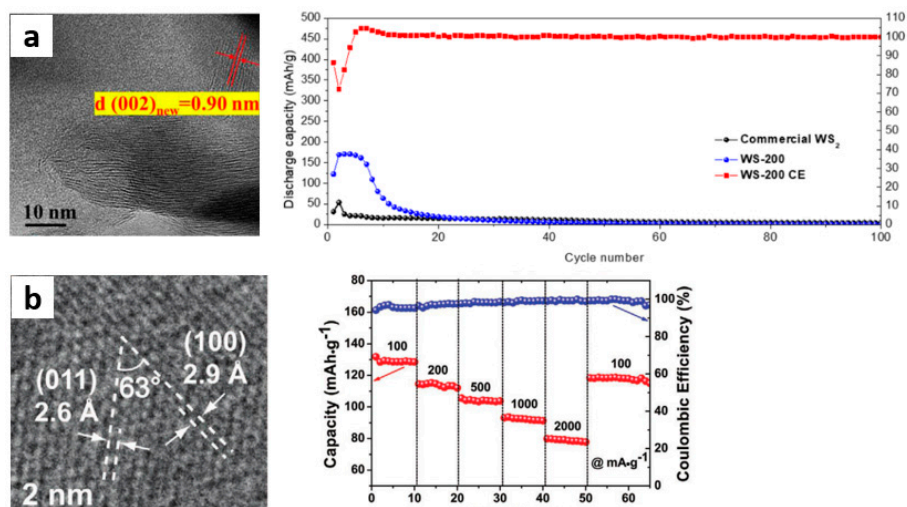


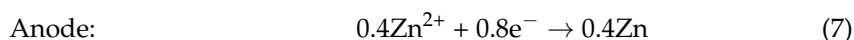
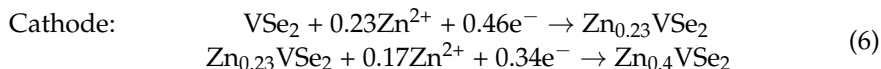
Figure 9. (a) HRTEM image, Cycling performances at current density of 200 mA g⁻¹ of WS-200 [51]; (b) HRTEM image and rate performance of VSe₂ [52].

In order to improve the electrochemical performance of WS₂, a modification strategy similar to MoS₂ and VS₂ can be designed to modify WS₂, the most important of which is hybridization and intercalation. For example, Debela et al. [80] synthesized WS₂@NGr material by hybridizing WS₂ with nitrogen-doped graphite. The reversible capacity of WS₂@NGr electrode reached 963 mAh·g⁻¹. Ratha et al. [81] synthesized layered WS₂ and reduced graphene oxide (RGO) hybrid materials by a simple hydrothermal method. WS₂/RGO composites showed excellent cycle stability in supercapacitors. Liu et al. [82] successfully synthesized a highly stable 1T-WS₂ nanobelt with a special zigzag chain superlattice structure. The NH₄⁺ insertion not only extends the interlayer spacing of WS₂ to 0.95 nm, but also makes the structure highly stable. Although the above three WS₂ modified materials are not applied to ZIB, they also provide many strategies. Starting from the microstructure of WS₂ and the storage mechanism of Zn²⁺ in WS₂, the carbon-based

materials and WS_2 can be hybridized, or external ions, such as NH_4^+ and crystal water, can be used for intercalation, so as to overcome the challenge of rapid capacity decline faced by WS_2 .

3.4. Other Materials

VSe_2 is also a typical layered structure, and the vanadium layer is alternately located between two selenium layers, forming a sandwich structure formed by van der Waals interaction [83,84]. Larger interlayer spacing (0.611 nm) provides sufficient transport channels and active sites for active cations. Moreover, the electronic coupling force between adjacent V^{4+} - V^{4+} induces metal properties and excellent electronic conductivity, making it an attractive candidate electrode material [85,86]. Wu et al. [52] prepared ultra-thin VSe_2 nanosheets and used them as cathode materials for ZIB. As shown in Figure 9b, the specific capacities of VSe_2 are 250.6 and 132.6 $\text{mAh}\cdot\text{g}^{-1}$ at 200 and 5000 $\text{mA}\cdot\text{g}^{-1}$, respectively. After 800 cycles at 2 $\text{A}\cdot\text{g}^{-1}$, the capacity retention was 83%. The factors influencing the excellent electrochemical performance of VSe_2 nanosheets cathode are attributed as follows: (1) Highly reversible Zn^{2+} intercalation/deintercalation storage mechanism; (2) Thanks to its ultra-thin two-dimensional morphology, Zn^{2+} has rapid diffusion kinetics ($D_{\text{Zn}^{2+}} \approx 10^{-8} \text{ cm}^2 \text{ s}^{-1}$); (3) The metal characteristics of VSe_2 are conducive to the thermodynamics and kinetics of Zn^{2+} storage process; (4) Stability of crystal structure of VSe_2 electrode material during long cycle. They summarized the storage mechanism of VSe_2/Zn battery as 6 and 7:



A few other TMD materials can also be used in the water-based zinc ion battery. For example, Zhang et al. [87] proved that CoS_2 could be used as anode material for a sulfur redox type non-aqueous zinc battery. Li et al. [88] synthesized a novel pre-cured titanium disulfide ($\text{Na}_{0.14}\text{TiS}_2$) as anode material for ZIB. However, these materials are all anode materials for ZIB, which are not described too much here.

4. Conclusions and Future Work

Since ZIB offer good safety and environmental protection, and with the deepening research on ZIB, they are expected to become a substitute for LIB. The special layered structure of TMDs is conducive to the transport of carriers such as Zn^{2+} . The nanoflower-like structure synthesized by the ordered stacking of monolayers confers TMD materials with a larger specific surface area. Some TMDs also have interlayer spacing larger than the diameter of hydrated zinc ion. Therefore, TMD materials are considered to represent a candidate cathode of ZIB with significant potential. Although TMDs are conducive, they also face the challenges of low reversible capacity and rapid capacity decay.

In recent years, some studies have reported that the modified TMD materials have excellent reversible capacity and cycle stability as cathodes of ZIB. Based on these research reports, the research progress of typical TMDs materials, such as MoS_2 , VS_2 , WS_2 , and VSe_2 , as cathodes of ZIB was described in this paper. The reversible capacity and long-period cycle performance are summarized in Table 2 and compared. At the same time, the modification ideas of TMD cathode materials for ZIB were combed, and the corresponding modification methods were summarized and discussed: (1) defect engineering, providing more ion storage sites and active sites by constructing chemical defects; (2) interlayer engineering, namely through the intercalation of guest ions to expand the layer spacing; (3) hybridization with carbon-based materials or other materials, making the microstructure of the composites more stable or maintained in a stable phase structure; (4) phase engineering, controlling the mutual transformation between 1H and 2R phases to reduce the diffusion energy barrier of Zn^{2+} and make the structure more stable; (5) in-situ

electrochemical oxidation, without changing the position of ions in the interlayer, where the low-valent active substances are oxidized into kinetic high-valent active substances by electrochemistry.

Table 2. Summary of the electrochemical performance of TMDs as ZIBs cathode.

Cathode Material	Electrolyte	Voltage	Capacity [mAh•g ⁻¹]	Cycle Stability	Ref
MoS ₂ -O	3M Zn (CF ₃ SO ₃) ₂	0.2–1.4V	232 at 0.1 A g ⁻¹	68% after 2000 cycles at 1.0 A g ⁻¹	[40]
E- MoS ₂	2M Zn (CF ₃ SO ₃) ₂	0.3–1.5V	202.6 at 0.1 A g ⁻¹	98.6% after 600 cycles at 1.0 A g ⁻¹	[39]
MoS ₂ /PANI	3M Zn (CF ₃ SO ₃) ₂	0.2–1.3V	181.6 at 0.1 A g ⁻¹	86% after 1000 cycles at 1.0 A g ⁻¹	[42]
MoS ₂ @CNTs	3M Zn (CF ₃ SO ₃) ₂	0.3–1.2V	180 at 0.1 A g ⁻¹	80.1% after 500 cycles at 1.0 A g ⁻¹	[43]
MoS ₂ -160	3M Zn (CF ₃ SO ₃) ₂	0.25–1.25V	168 at 0.1 A g ⁻¹	98.1% after 400 cycles at 1.0 A g ⁻¹	[44]
MoS ₂ ·nH ₂ O	3M Zn (CF ₃ SO ₃) ₂	0.2–1.25V	165 at 0.1 A g ⁻¹	88% after 800 cycles at 2.0 A g ⁻¹	[41]
MoS _{2-x}	3M Zn (CF ₃ SO ₃) ₂	0.25–1.25V	138.6 at 0.1 A g ⁻¹	87.8% after 1000 cycles at 1.0 A g ⁻¹	[38]
VS ₂ ·NH ₃	2M Zn (CF ₃ SO ₃) ₂	0.2–1.7V	390 at 0.1 A g ⁻¹	110% after 2000 cycles at 3.0 A g ⁻¹	[49]
VS ₂ /VO _x	25M ZnCl ₂	0.1–1.8V	260 at 0.1 A g ⁻¹	75% after 3000 cycles at 1.0 A g ⁻¹	[50]
rGO-VS ₂	3M Zn (CF ₃ SO ₃) ₂	0.4–1.7V	238 at 0.1 A g ⁻¹	93% after 1000 cycles at 5.0 A g ⁻¹	[47]
VS ₂ @SS	1M ZnSO ₄	0.4–1.0V	187 at 0.1 A g ⁻¹	80% after 2000 cycles at 2.0 A g ⁻¹	[46]
VS ₂ @VOOH	3M Zn (CF ₃ SO ₃) ₂	0.4–1.0V	165 at 0.1 A g ⁻¹	86% after 200 cycles at 0.5 A g ⁻¹	[48]
VS ₂	1M ZnSO ₄	0.4–1.0V	159.1 at 0.1 A g ⁻¹	98% after 200 cycles at 0.5 A g ⁻¹	[45]
WS-200	1M ZnSO ₄	0.1–1.5V	206.25 at 0.1 A g ⁻¹	0% after 100 cycles at 0.2 A g ⁻¹	[51]
VSe ₂	2M ZnSO ₄	0.1–1.6V	131.8 at 0.1 A g ⁻¹	80.8% after 500 cycles at 0.1 A g ⁻¹	[52]

Although these modification strategies are currently only applied to MoS₂ and VS₂, they should also be applicable to other TMD materials because the TMDs have similar special layered structures. For example, in view of the rapid decline of WS₂ capacity, we may venture to assume that the hybridization of WS₂ and carbon-based materials improves the structural stability of the composites, thus improving the poor cycle stability of WS₂ electrodes. With the modification strategies put forward, TMD materials are bound to receive more attention, and more series members of TMDs will become excellent cathode materials for ZIB.

Author Contributions: Conceptualization, T.L. and Y.X.; software, T.L. and J.Y.; validation, H.L., Y.X., and A.S.; investigation, T.L. and H.L.; resources, A.S. and Y.L.; data curation, T.L.; writing—original draft preparation, T.L.; writing—review and editing, A.S.; supervision, A.S.; funding acquisition, A.S. All authors have read and agreed to the published version of the manuscript.

Funding: This research was funded by the Hunan Provincial Natural Science Foundation (2021JJ30215), the Scientific Research Project of Hunan Provincial Department of Education (21A0363) and the Education Reform Project in Colleges and Universities of Hunan Province (HNJG-2020-0572).

Institutional Review Board Statement: Not applicable.

Informed Consent Statement: Not applicable.

Data Availability Statement: Not applicable.

Conflicts of Interest: The authors declare no conflict of interest.

References

1. Yan, H.; Zhang, X.; Yang, Z.; Xia, M.; Xu, C.; Liu, Y.; Yu, H.; Zhang, L.; Shu, J. Insight into the electrolyte strategies for aqueous zinc ion batteries. *Coord. Chem. Rev.* **2021**, *452*, 214297. [[CrossRef](#)]
2. Yang, S.; Cheng, Y.; Xiao, X.; Pang, H. Development and application of carbon fiber in batteries. *Chem. Eng. J.* **2020**, *384*, 123294. [[CrossRef](#)]
3. Wang, J.; Yang, Y.; Zhang, Y.; Li, Y.; Sun, R.; Wang, Z.; Wang, H. Strategies towards the challenges of zinc metal anode in rechargeable aqueous zinc ion batteries. *Energy Storage Mater.* **2020**, *35*, 19. [[CrossRef](#)]
4. Zhou, H.; Li, X.; Li, Y.; Zheng, M.; Pang, H. Applications of M_xSe_y ($M = Fe, Co, Ni$) and their composites in electrochemical energy storage and conversion. *Nano-Micro Lett.* **2019**, *11*, 40. [[CrossRef](#)] [[PubMed](#)]
5. Xiao, X.; Zou, L.; Pang, H.; Xu, Q. Synthesis of micro/nanoscaled metal-organic frameworks and their direct electrochemical applications. *Chem. Soc. Rev.* **2020**, *49*, 301. [[CrossRef](#)]
6. Hua, Y.; Li, X.; Chen, C.; Pang, H. Cobalt Based metal-organic frameworks and their derivatives for electrochemical energy conversion and storage. *Chem. Eng. J.* **2019**, *370*, 37. [[CrossRef](#)]
7. Zhang, N.; Xiao, X.; Pang, H. Transition metal (Fe, Co, Ni) fluoride-based materials for electrochemical energy storage. *Nanoscale Horiz.* **2019**, *4*, 99. [[CrossRef](#)]
8. Wang, F.; Liu, Y.; Zhao, Y.; Wang, Y.; Wang, Z.; Zhang, W.; Ren, F. Facile synthesis of two-dimensional porous $MgCo_2O_4$ nanosheets as anode for lithium-ion batteries. *Appl. Sci.* **2017**, *8*, 22. [[CrossRef](#)]
9. Qi, S.; Wu, D.; Dong, Y.; Liao, J.; Foster, C.W.; O'Dwyer, C.; Feng, Y.; Liu, C.; Ma, J. Cobalt-based electrode materials for sodium-ion batteries. *Chem. Eng. J.* **2019**, *370*, 185. [[CrossRef](#)]
10. Zheng, M.; Chi, Y.; Hu, Q.; Tang, H.; Jiang, X.; Zhang, L.; Zhang, S.; Pang, H.; Xu, Q. Carbon nanotube-based materials for lithium-sulfur batteries. *J. Mater. Chem. A* **2019**, *7*, 17204. [[CrossRef](#)]
11. Sharma, L.; Gond, R.; Senthilkumar, B.; Roy, A.; Barpanda, P. Fluorophosphates as efficient bifunctional electrocatalysts for metal air batteries. *ACS Catal.* **2020**, *10*, 43. [[CrossRef](#)]
12. Ru, Y.; Zheng, S.; Xue, H.; Pang, H. Potassium cobalt hexacyanoferrate nanocubic assemblies for high performance aqueous aluminum ion batteries. *Chem. Eng. J.* **2020**, *382*, 122853. [[CrossRef](#)]
13. Wrogemann, J.M.; Künne, S.; Heckmann, A.; Rodríguez-Pérez, I.A.; Siozios, V.; Yan, B.; Li, J.; Winter, M.; Beltrop, K.; Placke, T. Development of safe and sustainable dual ion batteries through hybrid aqueous/nonaqueous electrolytes. *Adv. Energy Mater.* **2020**, *10*, 1902709. [[CrossRef](#)]
14. Zeng, X.; Hao, J.; Wang, Z.; Mao, J.; Guo, Z. Recent progress and perspectives on aqueous zn-based rechargeable batteries with mild aqueous electrolytes. *Energy Storage Mater.* **2019**, *20*, 410. [[CrossRef](#)]
15. Kasiri, G.; Glenneberg, J.; Hashemi, A.B.; Kun, R.; Mantia, F.L. Mixed copper-zinc hexacyanoferrates as cathode materials for aqueous zinc-ion batteries. *Energy Storage Mater.* **2019**, *19*, 360. [[CrossRef](#)]
16. Jin, T.; Ji, X.; Wang, P.; Zhu, K.; Zhang, J.; Cao, L.; Chen, L.; Cui, C.; Deng, T.; Liu, S.; et al. High energy aqueous sodium-ion batteries. *Angew. Chem. Int. Ed.* **2021**, *60*, 11943–11948. [[CrossRef](#)]
17. Zhu, K.; Li, Z.; Jin, T.; Jiao, L. Low defects potassium cobalt hexacyanoferrate as a superior cathode for aqueous potassium ion batteries. *J. Mater. Chem. A* **2020**, *8*, 21103–21109. [[CrossRef](#)]
18. Pang, Q.; Yang, S.; Yu, X.; He, W.; Zhang, S.; Tian, Y.; Xing, M.; Fu, Y.; Luo, X. Realizing reversible storage of trivalent aluminum ions using $VOPO_4 \cdot 2H_2O$ nanosheets as cathode material in aqueous aluminum metal batteries. *J. Alloy. Compd.* **2021**, *885*, 161008. [[CrossRef](#)]
19. Shi, Z.; Wu, J.; Ni, M.; Guo, Q.; Zan, F.; Xia, H. Superior performance of calcium birnessite by electrochemical conversion as cathode for aqueous calcium ion battery. *Mater. Res. Bull.* **2021**, *144*, 111475. [[CrossRef](#)]
20. Fang, G.; Zhou, J.; Pan, A.; Liang, S. Recent advances in aqueous zinc ion batteries. *ACS Energy Lett.* **2018**, *3*, 2480–2501. [[CrossRef](#)]
21. Konarov, A.; Voronina, N.; Jo, J.H.; Bakenov, Z.; Sun, Y.; Myung, S. Present and future perspective on electrode materials for rechargeable zinc-ion batteries. *ACS Energy Lett.* **2018**, *3*, 2620–2640. [[CrossRef](#)]
22. Ming, J.; Guo, J.; Xia, C.; Wang, W.; Alshareef, H.N. Zinc-ion batteries: Materials, mechanisms, and applications. *Mater. Sci. Eng. R Rep.* **2019**, *135*, 58–84. [[CrossRef](#)]
23. Zhang, T.; Tang, Y.; Fang, G.; Zhang, C.; Zhang, H.; Guo, X.; Cao, X.; Zhou, J.; Pan, A.; Liang, S. Electrochemical activation of manganese based cathode in aqueous Zinc-Ion electrolyte. *Adv. Funct. Mater.* **2020**, *30*, 2002711. [[CrossRef](#)]
24. Ding, J.; Gao, H.; Ji, D.; Zhao, K.; Wang, S.; Cheng, F. Vanadium-based cathodes for aqueous zinc-ion batteries: From crystal structures, diffusion channels to storage mechanisms. *J. Mater. Chem. A* **2021**, *9*, 5258–5275. [[CrossRef](#)]
25. Cao, T.; Zhang, F.; Chen, M.; Shao, T.; Li, Z.; Xu, Q.; Cheng, D.; Liu, H.; Xia, Y. Cubic manganese potassium hexacyanoferrate regulated by controlling of the water and defects as a high capacity and stable cathode material for rechargeable aqueous zinc-ion batteries. *ACS Appl. Mater. Interfaces* **2021**, *13*, 26924–26935. [[CrossRef](#)] [[PubMed](#)]
26. Lee, W.S.V.; Xiong, T.; Wang, X.; Xue, J. Unraveling MoS_2 and transition metal dichalcogenides as functional zinc-ion battery cathode: A perspective. *Small Methods* **2020**, *5*, 2000815. [[CrossRef](#)] [[PubMed](#)]

27. Wu, J.; Ciucci, F.; Kim, J.-K. Molybdenum disulfide based nanomaterials for rechargeable batteries. *Chem. Eur. J.* **2020**, *26*, 6296–6319. [[CrossRef](#)] [[PubMed](#)]
28. Zhao, X.; Sui, J.; Li, F.; Fang, H.; Wang, H.; Li, J.; Cai, W.; Cao, G. Lamellar MoSe₂ nanosheets embedded with MoO₂ nanoparticles: Novel hybrid nanostructures promoted excellent performances for lithium ion batteries. *Nanoscale* **2016**, *8*, 17902–17910. [[CrossRef](#)] [[PubMed](#)]
29. Wang, L.; Xu, Z.; Wang, W.; Bai, X. Atomic mechanism of dynamic electrochemical lithiation processes of MoS₂ nanosheets. *J. Am. Chem. Soc.* **2014**, *136*, 6693–6697. [[CrossRef](#)]
30. Zhang, G.; Liu, H.; Qu, J.; Li, J. Two-dimensional layered MoS₂: Rational design, properties and electrochemical applications. *Energy Environ. Sci.* **2016**, *9*, 1190. [[CrossRef](#)]
31. Kuc, A.; Heine, T. The electronic structure calculations of two-dimensional transition-metal dichalcogenides in the presence of external electric and magnetic fields. *Chem. Soc. Rev.* **2015**, *44*, 2603. [[CrossRef](#)] [[PubMed](#)]
32. Jiao, Y.; Hafez, A.M.; Cao, D.; Mukhopadhyay, A.; Ma, Y.; Zhu, H. Metallic MoS₂ for high performance energy storage and energy conversion. *Small* **2018**, *14*, 1800640. [[CrossRef](#)]
33. Wu, D.; Wang, C.; Wu, M.; Chao, Y.; He, P.; Ma, J. Porous bowl-shaped VS₂ nanosheets/graphene composite for high rate lithium-ion storage. *J. Energy Chem.* **2020**, *43*, 24–32. [[CrossRef](#)]
34. Jing, P.; Lu, H.; Yang, W.; Cao, Y. Interlayer-expanded and binder-free VS₂ nanosheets assemblies for enhanced Mg²⁺ and Li⁺/Mg²⁺ hybrid ion storage. *Electrochim. Acta* **2020**, *330*, 135263–135272. [[CrossRef](#)]
35. Zhu, J.; Jian, T.; Wu, Y.; Ma, W.; Lu, Y.; Sun, L.; Meng, F.; Wang, B.; Cai, F.; Gao, J.; et al. A highly stable aqueous Zn/VS₂ battery based on an intercalation reaction. *Appl. Surf. Sci.* **2021**, *544*, 148882. [[CrossRef](#)]
36. Kim, H.J.; Choi, B.K.; Lee, I.H.; Kim, M.J.; Chun, S.; Jozwiak, C.; Bostwick, A.; Rotenberg, E.; Chang, Y.J. Electronic structure and charge-density wave transition in monolayer VS₂. *Curr. Appl. Phys.* **2021**, *30*, 8–13. [[CrossRef](#)]
37. Liu, J.; Peng, W.; Li, Y.; Zhang, F.; Fan, X. A VS₂@N-doped carbon hybrid with strong interfacial interaction for high-performance rechargeable aqueous Zn-ion batteries. *J. Mater. Chem. C* **2021**, *9*, 6308–6315. [[CrossRef](#)]
38. Xu, W.; Sun, C.; Zhao, K.; Cheng, X.; Rawal, S.; Xu, Y.; Wang, Y. Defect engineering activating (boosting) zinc storage capacity of MoS₂. *Energy Storage Mater.* **2019**, *16*, 527–534. [[CrossRef](#)]
39. Li, H.; Yang, Q.; Mo, F.; Liang, G.; Liu, Z.; Tang, Z.; Ma, L.; Liu, J.; Shi, Z.; Zhi, C. MoS₂ nanosheets with expanded interlayer spacing for rechargeable aqueous Zn-Ion batteries. *Energy Storage Mater.* **2019**, *19*, 94–101. [[CrossRef](#)]
40. Liang, H.; Cao, Z.; Ming, F.; Zhang, W.; Anjum, D.H.; Cui, Y.; Cavallo, L.; Alshareef, H.N. Aqueous Zinc-Ion storage in MoS₂ by tuning the intercalation energy. *Nano Lett.* **2019**, *19*, 3199. [[CrossRef](#)]
41. Zhang, Z.; Li, W.; Wang, R.; Li, H.; Yan, J.; Jin, Q.; Feng, P.; Wang, K.; Jiang, K. Crystal water assisting MoS₂ nanoflowers for reversible zinc storage. *J. Alloy. Compd.* **2021**, *872*, 159599. [[CrossRef](#)]
42. Huang, M.; Mai, Y.; Zhao, L.; Liang, X.; Fang, Z.; Jie, X. Tuning the kinetics of zinc ion in MoS₂ by polyaniline intercalation. *Electrochim. Acta* **2021**, *388*, 138624. [[CrossRef](#)]
43. Huang, M.; Mai, Y.; Zhao, L.; Liang, X.; Fang, Z.; Jie, X. Hierarchical MoS₂@CNTs hybrid as a long life and high rate cathode for aqueous rechargeable Zn-Ion batteries. *ChemElectroChem* **2020**, *7*, 4218–4223. [[CrossRef](#)]
44. Liu, J.; Xu, P.; Liang, J.; Liu, H.; Peng, W.; Li, Y.; Zhang, F.; Fan, X. Boosting aqueous zinc-ion storage in MoS₂ via controllable phase. *Chem. Eng. J.* **2020**, *389*, 124405. [[CrossRef](#)]
45. He, P.; Yan, M.; Zhang, G.; Sun, R.; Chen, L.; An, Q.; Mai, L. Layered VS₂ nanosheet based aqueous zn ion battery cathode. *Adv. Energy Mater.* **2017**, *7*, 1601920. [[CrossRef](#)]
46. Jiao, T.; Yang, Q.; Wu, S.; Wang, Z.; Chen, D.; Shen, D.; Liu, B.; Cheng, J.; Li, H.; Ma, L.; et al. Binder-free hierarchical VS₂ electrodes for high-performance aqueous zn ion batteries towards commercial level mass loading. *J. Mater. Chem. A* **2019**, *7*, 16330. [[CrossRef](#)]
47. Chen, T.; Chen, X.; Zhang, Q.; Li, Y.; Peng, W.; Zhang, F.; Fan, X. VS₂ nanosheets vertically grown on graphene as high-performance cathodes for aqueous zinc-ion batteries. *J. Power Sources* **2021**, *477*, 228652. [[CrossRef](#)]
48. Pu, X.; Song, T.; Tang, L.; Tao, Y.; Cao, T.; Xu, Q.; Liu, H.; Wang, Y.; Xia, Y. Rose-like vanadium disulfide coated by hydrophilic hydroxyvanadium oxide with improved electrochemical performance as cathode material for aqueous zinc-ion batteries. *J. Power Sources* **2019**, *437*, 226917. [[CrossRef](#)]
49. Yang, M.; Wang, Z.; Ben, H.; Zhao, M.; Luo, J.; Chen, D.; Lu, Z.; Wang, L.; Liu, C. Boosting the zinc ion storage capacity and cycling stability of interlayer-expanded vanadium disulfide through in-situ electrochemical oxidation strategy. *J. Colloid Interface Sci.* **2022**, *607*, 68–75. [[CrossRef](#)] [[PubMed](#)]
50. Yu, D.; Wei, Z.; Zhang, X.; Zeng, Y.; Wang, C.; Chen, G.; Shen, Z.X.; Du, F. Boosting Zn²⁺ and NH₄⁺ storage in aqueous media via in-situ electrochemical induced VS₂/VO_x heterostructures. *Adv. Funct. Mater.* **2021**, *31*, 2008743. [[CrossRef](#)]
51. Tang, B.; Tian, N.; Jiang, J.; Li, Y.; Yang, J.; Zhu, Q. Investigation of zinc storage capacity of WS₂ nanosheets for rechargeable aqueous zn-ion batteries. *J. Alloy. Compd.* **2022**, *894*, 162391. [[CrossRef](#)]
52. Wu, Z.; Lu, C.; Wang, Y.; Zhang, L.; Jiang, L.; Tian, W.; Cai, C.; Gu, Q.; Sun, Z.; Hu, L. Ultrathin VSe₂ nanosheets with fast ion diffusion and robust structural stability for rechargeable zinc-ion battery cathode. *Small* **2020**, *16*, 2000698. [[CrossRef](#)] [[PubMed](#)]
53. Liu, W.; Hao, J.; Xu, C.; Mo, J.; Dong, L.; Jiang, F.; Wu, J.; Kang, Z.; Jiang, B.; Kang, F. Investigation of zinc ion storage of transition metal oxides, sulfides, and borides in zinc ion battery systems. *Chem. Commun.* **2017**, *53*, 6872–6874. [[CrossRef](#)]

54. Chee, S.S.; Lee, W.J.; Jo, Y.R.; Cho, M.K.; Chun, D.; Baik, H.; Kim, B.J.; Yoon, M.H.; Lee, K.; Ham, M.H. Atomic vacancy control and elemental substitution in a monolayer molybdenum disulfide for high performance optoelectronic device arrays. *Adv. Funct. Mater.* **2020**, *30*, 1908147. [[CrossRef](#)]
55. Shu, H.; Zhou, D.; Li, F.; Cao, D.; Chen, X. Defect engineering in MoSe₂ for the hydrogen evolution reaction: From point defects to edges. *ACS Appl. Mater. Interfaces* **2017**, *9*, 42688–42698. [[CrossRef](#)]
56. Zhang, Y.; Tao, L.; Xie, C.; Wang, D.; Zou, Y.; Chen, R.; Wang, Y.; Jia, C.; Wang, S. Defect engineering on electrode materials for rechargeable batteries. *Adv. Mater.* **2020**, *32*, 1905923. [[CrossRef](#)]
57. Shao, Y.; Fang, Y.; Li, T.; Wang, Q.; Dong, Q.; Deng, Y.; Yuan, Y.; Wei, H.; Wang, M.; Gruverman, A.; et al. Grain boundary dominated ion migration in polycrystalline organic–inorganic halide perovskite films. *Energy Environ. Sci.* **2016**, *9*, 1752–1759. [[CrossRef](#)]
58. Zhou, J.; Lin, Z.; Ren, H.; Duan, X.; Shakir, I.; Huang, Y.; Duan, X. Layered intercalation materials. *Adv. Mater.* **2021**, *33*, 2004557. [[CrossRef](#)]
59. Cataldo, S.; Salice, P.; Menna, E.; Pignataro, B. Carbon nanotubes and organic solar cells. *Energy Environ. Sci.* **2012**, *5*, 5919–5940. [[CrossRef](#)]
60. Wang, Y.; Shi, Z.; Huang, Y.; Ma, Y.; Wang, C.; Chen, M.; Chen, Y. Supercapacitor devices based on graphene materials. *J. Phys. Chem. C* **2009**, *113*, 13103–13107. [[CrossRef](#)]
61. Leng, K.; Chen, Z.; Zhao, X.; Tang, W.; Tian, B.; Nai, C.T.; Zhou, W.; Loh, K.P. Phase restructuring in transition metal dichalcogenides for highly stable energy storage. *ACS Nano* **2016**, *10*, 9208. [[CrossRef](#)] [[PubMed](#)]
62. Fan, X.; Xu, P.; Li, Y.C.; Zhou, D.; Sun, Y.; Nguyen, M.A.; Terrones, M.; Mallouk, T.E. Controlled exfoliation of MoS₂ crystals into trilayer nanosheets. *J. Am. Chem. Soc.* **2016**, *138*, 5143–5149. [[CrossRef](#)] [[PubMed](#)]
63. Tang, Q.; Jiang, D. Mechanism of hydrogen evolution reaction on 1T-MoS₂ from first principles. *ACS Catal.* **2016**, *6*, 4953–4961. [[CrossRef](#)]
64. Lei, Z.; Zhan, J.; Tang, L.; Zhang, Y.; Wang, Y. Recent development of metallic (1T) phase of Molybdenum disulfide for energy conversion and storage. *Adv. Energy Mater.* **2018**, *8*, 1703482. [[CrossRef](#)]
65. Wang, R.; Yu, Y.; Zhou, S.; Li, H.; Wong, H.; Luo, Z.; Gan, L.; Zhai, T. Strategies on phase control in transition metal dichalcogenides. *Adv. Funct. Mater.* **2018**, *28*, 1802473. [[CrossRef](#)]
66. Tan, C.; Luo, Z.; Chaturvedi, A.; Cai, Y.; Du, Y.; Gong, Y.; Huang, Y.; Lai, Z.; Zhang, X.; Zheng, L.; et al. Preparation of high percentage 1T-Phase transition metal dichalcogenide nanodots for electrochemical hydrogen evolution. *Adv. Mater.* **2018**, *30*, 1705509. [[CrossRef](#)]
67. Jing, Y.; Zhou, Z.; Cabrera, C.R.; Chen, Z. Metallic VS₂ Monolayer: A promising 2D anode material for lithium ion batteries. *J. Phys. Chem. C* **2013**, *117*, 25409. [[CrossRef](#)]
68. Raccichini, R.; Varzi, A.; Passerini, S.; Scrosati, B. The role of graphene for electrochemical energy storage. *Nat. Mater.* **2015**, *14*, 271–279. [[CrossRef](#)] [[PubMed](#)]
69. Keyu, X.; Kai, Y.; Xin, L.; Wei, L.; Chao, S.; Chenglu, L.; Robert, V.; Pulickel, A.; Bingqing, W. Superior potassium ion storage via vertical MoS₂ “Nano-Rose” with expanded interlayers on graphene. *Small* **2017**, *13*, 1701471.
70. Xiang, T.; Fang, Q.; Xie, H.; Wu, C.; Wang, C.; Zhou, Y.; Liu, D.; Chen, S.; Khalil, A.; Tao, S.; et al. Vertical 1T-MoS₂ nanosheets with expanded interlayer spacing edged on a graphene frame for high rate lithium-ion batteries. *Nanoscale* **2017**, *9*, 6975–6983. [[CrossRef](#)]
71. Liu, H.; Zhang, F.; Li, W.; Zhang, X.; Lee, C.-S.; Wang, W.; Tang, Y. Porous tremella-like MoS₂/polyaniline hybrid composite with enhanced performance for lithium-ion battery anodes. *Electrochim. Acta* **2015**, *167*, 132. [[CrossRef](#)]
72. Prabhu, P.; Jose, V.; Lee, J.M. Design strategies for development of TMD-Based heterostructures in electrochemical energy systems. *Matter* **2020**, *2*, 526. [[CrossRef](#)]
73. Chen, Y.; Song, B.; Tang, X.; Lu, L.; Xue, J. Ultrasmall Fe₃O₄ nanoparticle/MoS₂ nanosheet composites with superior performances for lithium ion batteries. *Small* **2014**, *10*, 1536. [[CrossRef](#)] [[PubMed](#)]
74. Luo, H.; Wang, B.; Wang, F.; Yang, J.; Wu, F.; Ning, Y.; Zhou, Y.; Wang, D.; Liu, H.; Dou, S. Anodic oxidation strategy toward structure-optimized V₂O₃ cathode via electrolyte regulation for Zn-Ion storage. *ACS Nano* **2020**, *14*, 7328–7337. [[CrossRef](#)] [[PubMed](#)]
75. Ding, J.; Gao, H.; Zhao, K.; Zheng, H.; Zhang, H.; Han, L.; Wang, S.; Wu, S.; Fang, S.; Cheng, F. In-situ electrochemical conversion of vanadium dioxide for enhanced zinc-ion storage with large voltage range. *J. Power Sources* **2021**, *487*, 229369. [[CrossRef](#)]
76. Ding, J.; Du, Z.; Li, B.; Wang, L.; Wang, S.; Gong, Y.; Yang, S. Unlocking the potential of disordered rocksalts for aqueous zinc-ion batteries. *Adv. Mater.* **2019**, *31*, 1904369. [[CrossRef](#)]
77. Cao, Z.; Zhang, H.; Ge, Y.; Clemente, R.; Dong, P.; Wang, L.; Shen, J.; Ye, M.; Ajayan, P.M. An in situ electrochemical oxidation strategy for formation of nanogrid-shaped V₃O₇·H₂O with enhanced zinc storage properties. *J. Mater. Chem. A* **2019**, *7*, 25262. [[CrossRef](#)]
78. Georgiou, T.; Jalil, R.; Belle, B.D.; Britnell, L.; Gorbachev, R.V.; Morozov, S.V.; Kim, Y.-J.; Gholinia, A.; Haigh, S.J.; Makarovskiy, O.; et al. Vertical field-effect transistor based on graphene–WS₂ heterostructures for flexible and transparent electronics. *Nat. Nanotechnol.* **2013**, *8*, 100–103. [[CrossRef](#)] [[PubMed](#)]
79. Braga, D.; Lezama, I.G.; Berger, H.; Morpurgo, A.F. Quantitative determination of the band gap of WS₂ with ambipolar ionic liquid-gated transistors. *Nano Lett.* **2012**, *12*, 5218–5223. [[CrossRef](#)]

80. Debela, T.T.; Lim, Y.R.; Seo, H.W.; Kwon, I.S.; Kwak, I.H.; Park, J.; Cho, W.I.; Kang, H.S. Two-Dimensional WS₂@Nitrogen-Doped graphite for high-performance lithium ion batteries: Experiments and molecular dynamics simulations. *ACS Appl. Mater. Interfaces* **2018**, *10*, 37928–37936. [[CrossRef](#)] [[PubMed](#)]
81. Ratha, S.; Rout, C.S. Supercapacitor electrodes based on layered tungsten disulfide reduced graphene oxide hybrids synthesized by a facile hydrothermal method. *ACS Appl. Mater. Interfaces* **2013**, *5*, 11427–11433. [[CrossRef](#)] [[PubMed](#)]
82. Liu, Q.; Li, X.; Xiao, Z.; Zhou, Y.; Chen, H.; Khalil, A.; Xiang, T.; Xu, J.; Chu, W.; Wu, X.; et al. Stable metallic 1T-WS₂ nanoribbons intercalated with ammonia ions: The correlation between structure and electrical/optical properties. *Adv. Mater.* **2015**, *27*, 4837–4844. [[CrossRef](#)] [[PubMed](#)]
83. Lv, R.T.; Robinson, J.A.; Schaak, R.E.; Sun, D.; Sun, Y.F.; Mallouk, T.E.; Terrones, M. Transition metal dichalcogenides and beyond: Synthesis, properties, and applications of single and few-layer nanosheets. *Acc. Chem. Res.* **2015**, *48*, 56. [[CrossRef](#)]
84. Ma, Y.D.; Dai, Y.; Guo, M.; Niu, C.W.; Zhu, Y.T.; Huang, B.B. Evidence of the existence of magnetism in pristine VX₂ Monolayers (X = S, Se) and their strain-induced tunable magnetic properties. *ACS Nano* **2012**, *6*, 1695. [[CrossRef](#)] [[PubMed](#)]
85. Xu, K.; Chen, P.; Li, X.; Wu, C.; Guo, Y.; Zhao, J.; Wu, X.; Xie, Y. Ultrathin Nanosheets of Vanadium Diselenide: A Metallic Two-Dimensional Material with Ferromagnetic Charge-Density-Wave Behavior. *Angew. Chem. Int. Ed.* **2013**, *52*, 10477. [[CrossRef](#)]
86. Yang, J.R.F.; Lv, F.; Zhou, J.H.; Lin, C.F.; Wang, K.; Zhang, Y.L.; Yang, Y.; Wang, W.; Li, J.B.; Guo, S.J. Metallic graphene-like VSe₂ ultrathin nanosheets: Superior potassium-ion storage and their working mechanism. *Adv. Mater.* **2018**, *30*, 1800036. [[CrossRef](#)]
87. Zhang, R.X.; Pan, C.S.; Nuzzo, R.G.; Gewirth, A.A. CoS₂ as a sulfur redox-active cathode material for high-capacity nonaqueous Zn batteries. *J. Phys. Chem. C* **2019**, *123*, 8740. [[CrossRef](#)]
88. Li, W.; Wang, K.L.; Cheng, S.J.; Jiang, K. An ultrastable presodiated titanium disulfide anode for aqueous “Rocking-Chair” zinc ion battery. *Adv. Energy Mater.* **2019**, *9*, 1900993. [[CrossRef](#)]